The insulin / IGF axis is critically important controlling gene transcription in the podocyte.

Jennifer A. Hurcombe[1], Lusyan Dayalan[1], Fern Barrington[1], Frédéric Burdet[2], Lan Ni[1], Joseph T. Coward[1], Paul T. Brinkkoetter[3], Martin Holzenberger[4], Aaron Jeffries[5], Sebastian Oltean[6], Gavin I. Welsh[1], Richard J.M. Coward[1]

1. Bristol Renal, University of Bristol, Bristol, United Kingdom. 2.Vital-IT Systems Biology Division, SIB Swiss Institute of Bioinformatics, Lausanne, Switzerland. 3. University Hospital Cologne, Cologne, Germany. 4. INSERM and Sorbonne University, Paris, France. 5. Biosciences, Faculty of Health and Life Sciences, University of Exeter, Exeter, United Kingdom. 6. Department of Clinical and Biomedical Sciences, Medical School, University of Exeter, Exeter, United Kingdom

Corresponding author: Professor Richard Coward

Email: Richard.Coward@bristol.ac.uk – tel: +44 117 331 3117

Running title: Effects of simultaneous knockout of podocyte IR and IGF1R

Keywords: podocyte, insulin receptor, IGF1R, spliceosome, RNA processing

SUMMARY

Signalling to the podocyte via the structurally related insulin receptor (IR) or insulin-like growth factor 1 receptor (IGF1) is important for podocyte function. This study sought to elucidate the compound role of the insulin/IGF1 axis in podocytes using transgenic mice and cell culture models deficient in both receptors.

Podocyte specific IR/IGF1R knockdown mice developed a severe kidney phenotype with albuminuria, glomerulosclerosis and renal failure with death occurring in some mice between 4 and 24 weeks. Simultaneous knockdown of both receptors in cultured podocytes resulted in >50% cell death by 7 days.

Proteomic analysis revealed a striking downregulation of spliceosome-related proteins in IR/IGF1R knockdown podocytes with long-read RNA sequence data indicating an increased fraction of transcripts with intron retention/premature termination codons in these cells.

This work underlines the critical importance of podocyte insulin/IGF signalling revealing a novel role for this extrinsic hormonal signalling axis in regulating gene transcription.

INTRODUCTION

Podocytes are highly specialised, terminally differentiated epithelial cells located at the urinary aspect of the glomerular basement membrane (GBM) in the kidney. They are critical in maintaining glomerular filtration barrier integrity thus preventing the development of albuminuria, an independent risk factor for end-stage-kidney-disease [ESKD] (1), cardiovascular morbidity (2) and death. Therefore, understanding the critical signalling pathways necessary for maintaining podocyte health is desirable.

The insulin/insulin-like growth factor (IGF) signalling axis regulates many aspects of growth and metabolism: insulin signalling is predominantly associated with metabolism and IGF signalling with growth and cell division (3). However, insulin, IGF1 and their cognate receptors (the insulin receptor [IR] and insulin-like growth factor receptor [IGF1R]) share significant structural homology and several common downstream signalling nodes (4). The IR and IGF1R can bind each other's ligands and can act redundantly in some contexts (5, 6). The constitutive global (whole body) loss of either the IR or IGF1R in murine knockout models is lethal (7, 8) suggesting a limited ability for these receptors to compensate for each other in every cell type. However, it is now clear that the insulin / IGF axis has different roles in different cell types. Several mouse models with tissue-specific dual knockout of both the IR and IGF1R show differential consequences occurring in a cell type dependent manner (9-13).

Insulin signalling to the podocyte via the IR is critical for podocyte function (14-17) and it is apparent that IGF signalling is also important for podocyte homeostasis (18-20). Recently we have shown that loss of podocyte IGF1 signalling can have both detrimental and beneficial effects dependent upon the level of IGF1R suppression: whilst near total loss of podocyte IGF1R expression results in severe mitochondrial dysfunction associated with cell death, partial receptor inhibition promotes podocyte survival in conditions of cellular stress (21).

Here we show that combined simultaneous loss of both the IR and IGF1R in podocytes is physiologically highly detrimental and present proteomic and transcriptomic analyses indicating that the IR/IGF1R hormonal signalling axis is crucial in controlling spliceosome assembly and RNA processing in this cell.

METHODS

Mouse models

Mice in which exon four of the IR (7) and exon three of the IGF1R have been flanked by loxP sites (8) were crossed with podCre mice (22). Progeny with the genotype podCre $^{+/-}$ IR $^{wt/fl}$ IGF1R$^{wt/fl}$ was then crossed with IR$^{fl/fl}$ IGF1R$^{fl/fl}$ mice to generate podocyte specific IR/IGF1R knockdown animals from embryonic day 12 (podDKO) (Supp Figure 1A). Cre negative littermates served as controls. All mice were on a mixed genetic background including contributions from 129/Sv, FVB and C57BL/6. Both sexes were studied, and no phenotypic differences observed.

Transgenic mouse work was carried out in accordance with the University of Bristol's institutional guidelines, and procedures approved by the United Kingdom (UK) Home Office in accordance with UK legislation. (Home Office Protocol numbers PPL 3003394 & PPL 2012285).

Urinary albumin and creatinine measurements

Albumin and creatinine levels in spot collections of mouse urine were measured using a mouse-specific albumin ELISA (Universal Biologicals, Cat# E90-134) and creatinine companion kit (Exocell, Cat# 1012), following the manufacturer's methodology.

Histology and periodic acid-Schiff staining

Kidneys were fixed in 10% buffered neutral formalin, further processed and paraffin embedded. 3 µm sections were cut and stained using a Periodic acid-Schiff staining kit (Sigma) according to the manufacturer's instructions. Tissues were imaged using a Leica DN2000 microscope and micrographs taken using Leica Application Suite software. Image analysis was performed using ImageJ; all images were contrast enhanced using the same parameters.

Glomerulosclerosis was scored for each glomerulus as follows: 0=normal glomeruli; 1=up to 25% involvement; 2=25-50% involvement; 3=50-75% involvement; 4=over 75% involvement. The glomerulosclerosis index was calculated as described previously (23) and according to the formula [(1xN1)+(2xN2)+(3xN3)+(4xN4)]/(N0+N1+N2+N3+N4) were Nx is the number of glomeruli with each given score.

Electron microscopy

Tissues for electron microscopy were fixed in 0.1 M sodium cacodylate, 2% glutaraldehyde, and imaged on a Technai 12 transmission electron microscope. Average slit diaphragm, foot process and glomerular basement membrane width were calculated using ImageJ assessing at least 20 regions of glomerular basement membrane from at least 2 glomeruli per mouse.

Lentiviral transduction of a conditionally immortalised IR/IGF1R floxed podocyte cell line

Kidneys were isolated from IR $^{fl/fl}$ IGF1R$^{fl/fl}$ mice and used to make a temperature-sensitive SV40 conditionally immortalised podocyte cell line using techniques as described previously (24) (Figure S2). Podocytes were cultured at 33°C and when 50% confluent were thermo-switched to 37°C and incubated for a further 7 days before transduction with a lentivirus expressing Cre recombinase as described previously. Transduction was in RPMI media with hexadimethrine bromide (Sigma) at 4 µg/ml and the virus used at a multiplicity of infection of 1. Following a 24-hour incubation, the lentivirus was removed and replaced with fresh media. Cells were incubated for a further 3-7 days before imaging and protein extraction.

To determine ciDKO cell number, cells were washed 3 times in PBS, the nuclei stained with Hoechst (Sigma) at 1 µg/ml and imaged using an IN Cell analyser 2200 (GE Healthcare), and data analysed using IN Cell analyser Developer software (GE Healthcare).

Cell culture

Conditionally immortalised podocyte cell lines were cultured as described previously (25). For acute insulin and IGF1 stimulation, cells were serum starved for 4 hours, then 10 nM and 100 nM of insulin or 10 ng/ml and 100 ng/ml IGF1 was applied to the cells for 10 minutes. Spliceosome inhibitor treatment was carried out using pladienolide B at 0-100 nM for 48 hours before determination of cell number.

Western blotting

Cultured cells were lysed in radioimmunoprecipitation assay buffer supplemented with protease and phosphatase inhibitors (Sigma). 10-30 µg of protein was resolved by electrophoresis and then transferred to a polyvinylidene difluoride membrane (Millipore). Membranes were blocked in TRIS-buffered saline with 0.1% tween 20 and 5% BSA for 1 hour and then incubated overnight with primary antibody at a dilution of 1:1000. Membranes were washed before incubation with horseradish peroxidase conjugated secondary antibody (Sigma). Immunoreactive bands were visualised using Clarity ECL Western blotting substrate (Biorad) on a GE AI600 imager. Densitometry was performed using ImageJ software.

Proteomic analysis

ciDKO podocytes (3 days after Cre lentiviral transduction and before significant cell loss) were lysed in RIPA buffer and subjected to LC-MS/MS using isobaric TMT labelling as described previously (26, 27). n=9 ciDKO and control podocytes were analysed. Wild-type mouse podocytes served as controls.

The data output from Proteome Discoverer 2.1 was further analysed in Microsoft Office Excel, Graphpad Prism 9 and Perseus 1.6.10.43 using $\log_2$-transformed scaled total protein abundance data. A *t*-test was used to determine significantly differentially expressed proteins. Hierarchical clustering was performed in Perseus by Euclidean distance using *k*-means pre-processing. Gene

ontology (GO) and Kyoto Encyclopaedia of Genes and Genomes (KEGG) and enrichments were performed in Perseus using a Fisher test of significantly changed proteins versus the unchanged population after annotation with the proteins.

For Search Tool for the Retrieval of Interacting Genes/Proteins (STRING) enrichment analysis, the ciDKO expression dataset was submitted to STRING with $\log_2$ fold change values associated with each protein. Functional enrichments were identified, and enrichment scores calculated based on aggregate fold change or Kolmogorov-Smirnov testing in STRING.

Long read RNA sequencing

RNA was isolated from ciDKO podocytes (3 days after Cre lentiviral transduction) and wild-type control cells (n=4 for each group) using an RNeasy mini kit (Qiagen). RNA was quantified using a Qubit Fluorimeter (Thermo Fisher Scientific) and quality assessed using the TapeStation system (Agilent). All samples had an RNA integrity number >8.

Barcoded PCR-cDNA library preparation was performed on 75 ng of RNA from each sample using the SQK-PCB109 kit (Oxford Nanopore Technologies). The resulting library was quantified using a Qubit Fluorimeter (Thermo Fisher Scientific) and molecular weight estimated using the TapeStation system (Agilent). 50 fmol of library was then loaded onto three promethION R9.4.1 flowcells (Oxford Nanopore Technologies), sequenced for 72 h and basecalled using guppy_basecaller 5.0.17 (Oxford Nanopore Technologies) in high accuracy mode.

Long read RNA analysis

IsoQuant analysis: the reads were aligned using IsoQuant (version 2.3.0), with option --data_type nanopore. The mouse gencode annotation (V29) (28) was used. The IsoQuant reference-based transcripts counts were used for further analysis. Differential expression analysis between the 2 conditions was performed using limma function with voom approach from limma Bioconductor package (29). The transcripts were analyzed without being grouped by genes, which will lead to a more stringent analysis than if done by gene (multiple correction testing is done by transcript). For visualization in the genome browser, the bam files were converted to bigWig files (using a scaleFactor calculated with edgeR (30)). FLAIR analysis (flair version 1.6.4): pychopper (version 2.7.2) (31) was first run on the total reads. Then the full length and rescued reads were aligned with “flair align” on the reference fasta file. The alignments were corrected using “flair correct”. The alignments were then collapsed using “flair collapse”, using the 8 replicates, into 1 complete reference. Then flair quantify, diffExp and diffSplice were run using the 2x4 replicates to get the rank lists of the 4 splicing event types (cassette, 3’, 5’, IR). A custom R script was used to find the nearest gene to the splicing events. In parallel, flair mark_intron_retention and predictProductivity (option --longestORF) were run on each corrected alignments to list the intron retention events by sample and predict the transcripts productivity by sample.

Quantitative PCR

cDNA was synthesised from RNA isolated from ciDKO and wild-type podocytes using the High-Capacity RNA-to-cDNA kit (ThermoFisher Scientific). Quantitative PCR was performed using SYBR Green JumpStart Taq ReadyMix (Merck) in a StepOnePlus PCR machine (Applied Biosystems). Primers with the following sequences were purchased from Life Technologies: Fn1 F 5' CCCAGCTCACTGACCTAAGC 3'; Fn1 R 5' GGAAGAGTTTAGCGGGGTCC 3'; Hcfc1r1 F 5' GCCACCACTGGGGTAACTC 3'; Hcfc1r1 R 5'CTTCGGGAAAAGTCACAGGG3'; beta actin F 5' GACAGGATGCAGAAGGAGATTACT 3'; beta actin R 5' TGATCCACATCTGCTGGAAGGT 3'.

Statistical analysis

Statistical analysis was performed in Graphpad Prism 9 and data presented as the mean +/- SEM unless otherwise stated. Statistical significance was calculated with *t*-tests to compare two groups or one-way ANOVA to compare more than two groups and taken as $p<0.05$.

Data availability

The authors declare that all data supporting the findings of this study are available within the article and its supplementary information files or from the corresponding author upon reasonable request. The mass spectrometry proteomics data have been deposited in the PRIDE repository as part of the ProteomeXchange Consortium(32) under the dataset identifier PXD051018.

RESULTS

podDKO mice develop a severe renal phenotype by 24 weeks

To study the effect of the combined loss of podocyte IR and IGF1R *in vivo*, transgenic mice were generated by crossing $IR^{fl/fl}/IGF1R^{fl/fl}$ mice with mice expressing Cre recombinase under the control of a podocin promotor (Figure S1A). There was no difference in body weight or blood glucose in podDKO mice compared with littermate controls (Figures 1A and B). However, knockout mice developed albuminuria with significantly increased urinary albumin:creatinine ratio (uACR) ($p<0.01$) at 24 weeks of age (Figure 1C). The severity of the phenotype was variable and while some mice exhibited only mild albuminuria, more severe renal disease was observed in others resulting in death in ~20% of the mice. uACR was not increased in Cre negative and podCre expressing mice at 6 months excluding Cre toxicity as the driver of albuminuria in podDKO mice (Figure S1C). Glomerulosclerosis was significantly increased ($p<0.05$) in knockout mice with areas of sclerosis and tubular protein casts visible on periodic acid-Schiff (PAS) stained sections (Figure 1D), together with evidence of increased fibrosis as determined by Masson's trichrome staining (Figure 1E). Transmission electron microscopy (TEM) analysis revealed disruption of the filtration barrier ultrastructure with significantly increased ($p<0.01$) foot process width (Figure 1F). Podocyte number, evaluated by immunofluorescence (IF) using a podocyte specific WT1 antibody, was significantly ($p<0.0001$) reduced in podDKO mice (Figure 1G).

Simultaneous knockout of podocyte IR and IGF1R *in vitro* is highly detrimental

We surmised that the variable phenotype observed in our transgenic mouse model was due to differences in the efficiency of Cre mediated excision and level of receptor knockdown. With the aim of developing a model with near total loss of the IR and IGF1R to use in *in vitro* studies, a conditionally immortalised podocyte cell line was generated from $IR^{fl/fl}/IGF1R^{fl/fl}$ mice and these cells transduced with Cre expressing lentivirus (ciDKO) (Figure S2). This allowed us to initially culture the cells containing both receptors before their simultaneous deletion using Cre recombinase. Western blot analysis showed a decrease of the IR ($p<0.0001$) and IGF1R ($p<0.0001$) in ciDKO podocytes of >80% (Figure 2A). Phosphorylation of AKT and p44/42 MAPK in response to either acute insulin or IGF1 stimulation was reduced ($p<0.05$) indicating suppression of insulin/IGF1 signalling in ciDKO podocytes (Figures 2B and C). Compound loss of both the IR and IGF1R was detrimental, resulting in >50% podocyte loss ($p<0.0001$) 7 days after Cre-mediated gene excision (Figure 2D).

Proteomic analysis of ciDKO podocytes reveals downregulation of spliceosome proteins

To elucidate the mechanistic processes regulated by insulin/IGF1 signalling in podocytes, we performed unbiased tandem mass tagged (TMT) LC MS/MS proteomics to compare total protein expression in ciDKO compared with wild-type cells (Figure 3A). Hierarchical clustering and principal component analysis (PCA) was performed using Perseus software to determine that samples were clustered according to the experimental group (Figures S3A and S3B). 4842 proteins were significantly differentially expressed in ciDKO cells compared to wild-type controls with 2127 proteins upregulated and 2715 proteins downregulated (Figure 3A and Figure S3C). Perseus software was

used to perform hierarchical clustering and identify Gene Ontology (GO) and Kyoto Encyclopaedia of Genes and Genomes (KEGG) terms enriched in ciDKO podocytes (Figure 3B). This revealed a downregulation of proteins involved in DNA replication and cell cycling along with a striking downregulation of proteins involved in spliceosome function and RNA processing (Figure 3B). These findings were confirmed using Search Tool for the Retrieval of Interacting Genes/Proteins (STRING) to identify KEGG terms overrepresented in the ciDKO proteome (Figure 3C). STRING identified the spliceosome as the most significantly enriched KEGG term in dual receptor knockout cells with a $-\log_{10}$ false discovery rate ~2 fold greater than any other (Figure 3D).

To validate results from the proteomic data, western blot analysis of wild-type and ciDKO podocytes was performed using antibodies to selected spliceosome proteins. This confirmed that levels of eukaryotic initiation factor-4A (EIF4A) ($p<0.001$), splicing factor 3B subunit 4 (SF3B4) ($p<0.01$) and polypyrimidine tract binding protein 2 (PTBP2) ($p<0.05$) were significantly reduced in knockout cells (Figure 3E).

Exposure of cultured podocytes, but not glomerular endothelial cells, to the spliceosome inhibitor pladienolide B results in dose dependent cell death

Proteomic analysis indicated a significant reduction in spliceosome proteins associated with all stages of the splicing process in ciDKO podocytes (Figure 4A). We therefore hypothesised that impaired spliceosome assembly and function may be at least partially responsible for the deleterious phenotype observed with podocyte IR/IGF1R knockout. To determine the importance of spliceosome activity to mature podocyte homeostasis and to ascertain whether different cell types are equally sensitive to spliceosome inhibition, the cytotoxic effect of pladienolide B (a spliceosome inhibitor targeting SF3B) (33) was compared in HeLa cells, fully differentiated, wild-type murine podocytes and glomerular endothelial cells. Consistent with previous observations (33), exposure of HeLa cells to pladienolide B at 0-100 nM for 48 hours was cytotoxic at ≥1 nM (Figure 4B). Pladienolide B-induced spliceosome inhibition also resulted in a significant ($p<0.05$) dose dependent loss of podocytes at a concentration of ≥25 nM (Figure 4D and E). In contrast, no cytotoxicity was observed in glomerular endothelial cells (Figure 4C).

Loss of podocyte IR and IGF1R is associated with increases in intron retention and unproductive transcript expression

To obtain an overview of global differences in various alternative splicing events in the ciDKO transcriptome, long-read RNA sequencing was used. Long-read sequencing was preferred as short-read RNA seq tools have been found to detect such events with poor accuracy (34). RNA was isolated from ciDKO and wild-type control cells, sequenced using long-read RNA Oxford Nanopore PromethION flow cells (Figure 5A) and the resulting data analysed using the Full-Length Alternative Isoform Analysis of RNA (FLAIR) tool. An overview of the main types of alternative splicing events is depicted in Figure 5B and rank lists of genes in ciDKO podocytes with significantly increased (adjusted p value <0.05) intron retention splicing; alternative 5' splicing; alternative 3' splicing and cassette exon splicing are shown in Supp Tables 1-4. KEGG pathway enrichment analysis using

STRING, shows an overlap in overrepresented pathways (including Spliceosome, RNA transport and Ribosome) from rank lists of genes with intron retention, cassette exon splicing and alternative 5' splicing (Supp Figure 4D-F).

To compare the intron retention in the ciDKO versus controls, the number of intron retention events by sample were counted using FLAIR mark_intron_retention, and then divided by the number of transcripts per sample. The ciDKO samples have a significantly (p-value = 0.004) higher proportion of transcripts with intron retention: ~18% of transcripts in ciDKO podocytes compared with 14% in wild-type controls (Figure 5C). The overlap of the intron retention events between experimental repeats is ~30% in both wild-type and ciDKO podocytes. The transcript productivity was also assessed using FLAIR predictProductivity with transcripts classified in 4 categories: PRO (productive); PTC (premature termination codon, i.e. unproductive); NGO (no start codon) and NST (has start codon but no stop codon appended to the end of the isoform name). The fraction of transcripts harbouring a premature termination codon is significantly higher ($p<0.001$) in ciDKO podocytes (Figure 5D and E).

Compound knockdown of the IR and IGF1R alters the podocyte transcriptome

To determine the effect of spliceosome depletion on the transcriptomic profile of ciDKO podocytes, IsoQuant (35) was used to quantify genes and transcripts from existing GENCODE mouse annotation, then limma (29) used to determine differential gene and transcript expression. The number of reads per sample is shown in Figure S4A. Variance-stabilized transformed RNA Seq data (Figure S4 B) were used in principal component analysis and confirmed that samples were clustered according to the experimental group (Figure S4C). The number of minimally expressed transcripts in the experiment was 31580 and using an adjusted p-value threshold of 0.01, 831 transcripts were significantly upregulated and 570 significantly downregulated in ciDKO podocytes. The top 10 most significantly differentially expressed genes (analysed by transcript) are shown in Table 1. These included down-regulation of host cell factor C1 regulator 1 (Hcfc1r1), a nuclear export factor which regulates the activity of the transcription factor host cell factor 1 (Hcf1) and which analysis using FLAIR identified as subject to increased alternative 3' splicing in ciDKO podocytes (Supp Table 4). Also, fibronectin 1 (Fn1) encoding an extracellular matrix protein which exists as different isoforms derived by alternative splicing at three sites: Extra Domains A and B exons (EDA and EDB) and the type III connecting segment (36). Fn1 splice variants were differentially expressed in ciDKO podocytes with increased expression (log fold change of 1.11[=2.16 fold]) of an Fn1 transcript containing the EDA and EDB exons (Figure 6A-C). qPCR validation confirmed the decrease in Hcfc1r1 expression (Figure 6D) while primers designed to specifically amplify transcripts containing the fibrosis-associated Fn1 EDB exon also verified that expression of such transcripts is significantly increased (1.8 fold, $p<0.001$) in ciDKO podocytes when compared with wild-type control cells (Figure 6E).

DISCUSSION

We have previously shown that signalling to the podocyte via the IR is critical for kidney function (17) while the IGF1R has a role in maintaining podocyte mitochondrial function (21). The current study used *in vivo* and *in vitro* models lacking both receptors simultaneously to further elucidate important common signalling pathways regulated by the insulin/IGF1 axis in the podocyte.

We initially used a transgenic mouse model (podDKO) to determine the physiological consequences of dual receptor loss *in vivo*. These mice developed an obvious renal phenotype: significant albuminuria, glomerulosclerosis, and ultrastructural filtration barrier damage was apparent by 6 months and was severe enough to cause death in a number of mice. However, body weight and blood glucose in podDKO mice were comparable to controls, in contrast with several other mouse models where alongside tissue-specific manifestations, double receptor knockout also gives rise to systemic effects. For example, IR/IGF1R knockout in kidney proximal tubule cells (10) and muscle (11) both result in decreased body size while other models have impairments in systemic metabolism: mice with adipose tissue-specific IR/IGF1R knockout develop diabetes (9) while dual receptor knockout in hippocampus and central amygdala results in a decrease in glutamate receptors and reduced glucose tolerance (12).

We performed unbiased proteomic analysis to identify the mechanistic processes responsible for the detrimental phenotype observed in our *in vivo* and *in vitro* models. Given the well-established mitogenic effect of IGF1 signalling (37), this showed a predictable downregulation of cell cycle and DNA replication pathways. However, we also observed a decrease in DNA damage response pathways and histone methylation. As post-mitotic cells with a limited capacity for replenishment, maintaining genomic integrity is crucial for podocyte health (38-40). Furthermore, altered histone methylation, another feature of the podocyte IR/IGF1R knockdown proteome, has been shown to affect the function of the DNA repair system in podocytes (41). Recent studies suggest that podocyte DNA damage and changes in glomerular DNA methylation may be useful markers of chronic kidney disease and correlate with estimated glomerular filtration rate (eGFR) decline in patients with diabetic nephropathy (42). It therefore seems plausible that deficiencies in DNA damage repair mechanisms contribute to the detrimental phenotype and ultimate loss of podocytes resulting from IR/IGF1R knockdown.

Evidence from previous studies suggests that DNA damage is intrinsically linked with spliceosome function: DNA damage affects the expression, activity and localisation of splicing factors (43) while spliceosome dysfunction leads to DNA damage by promoting the aberrant formation of R loops during transcription (44, 45). Thus, accurate spliceosome function is critical for maintaining genomic integrity (44). In addition to the decreased expression of DNA damage response proteins revealed by our proteomic data, we also observed a striking reduction in the levels of proteins required for spliceosome assembly and regulation in ciDKO podocytes. We have previously used lentiviral mediated expression of Cre recombinase to induce knockout of other podocyte genes, notably glycogen synthase kinase 3 α and β in combination (27). While this resulted in a highly detrimental

cellular phenotype, proteomic analysis of these cells showed no differences in the expression of spliceosome related proteins, so we are confident that the results from the current study are not due to generalised cell death/dysfunction.

The spliceosome is a large ribonucleoprotein complex whose critical function in all eukaryotic cells is to catalyse the removal of introns from precursor messenger RNA molecules and join the flanking exons to generate mature mRNA transcripts that direct protein synthesis during translation (46). Spliceosome function is also a driver of significant proteomic diversity via alternative splicing, whereby multiple mRNA transcripts containing different exon combinations are produced from a single gene (46). Mutations in core spliceosome components, spliceosome assembly factors or regulatory proteins can result in defects in pre-RNA processing, increased nonsense-mediated decay of affected transcripts, abnormal or truncated protein products and changes to alternative splicing. Such erroneous splicing can substantially alter the transcriptome in specific cell types. This has been shown in immune cell dysfunction (47), cancer (47) and neurodegeneration (48, 49). Somatic mutations in genes encoding spliceosome components can result in diseases, known as spliceosomopathies, (including retinitis pigmentosa, myelodyplastic syndromes and craniofacial disorders (50)), with tissue-specific manifestations, suggesting that although spliceosome factors are ubiquitously expressed, they likely have cell type specific functions. Interestingly, one of the splice factors frequently involved in these spliceosomopathies - SF3B4 - is down regulated in the double knock-down podocytes (Figure 3E). We used the spliceosome inhibitor pladienolide B (51), which targets the SF3B complex, to investigate the effect of reduced spliceosome activity in wild-type podocytes. Developed as an anti-neoplastic agent, pladienolide B is effective at reducing cell viability, particularly in cancer cell lines (51-54), presumably due to an increased demand for translation and protein production in such actively dividing cells. In contrast, a comparatively high dose of pladienolide B is not sufficient to induce cytotoxicity in HEK 293T cells, suggesting that not all cell types are equally sensitive to spliceosome inhibition (55). While we were able to reproduce the low dose cytotoxic effect of this spliceosome inhibitor in HeLa cells reported previously (51), the response of the glomerular cell types we assayed differed. No cytotoxic effect was apparent in glomerular endothelial cells while in contrast, we found podocytes to be sensitive to pladienolide B, resulting in significant cell death and suggestive of the importance of adequate spliceosome function in this cell type. The splicing factor CD2 antigen cytoplasmic tail binding protein 2 (CD2BP2) is known to be essential for kidney development and podocyte integrity (56) while alternative splicing of genes including Wilm's tumour gene 1 (WT1) (57) and vascular endothelial growth factor A (VEGF-A) (58) is important in podocyte homeostasis and disruption of this tightly regulated process associated with chronic kidney disease (59). We therefore performed long-read RNA sequencing to explore the effect of podocyte IR/IGF1R loss on spliceosome function and the transcriptome of ciDKO cells.

Long read RNA Seq analysis shows that podocyte IR/IGF1R depletion has a marked impact on alternative splicing events, notably an increase in the fraction of transcripts with intron retention/premature termination codons. Interestingly, enrichment analysis shows that many transcripts associated with spliceosome function and RNA transport have increased levels of intron

retention, cassette exon splicing and alternative 5' and 3' splicing. Although it has recently been recognised that intron retention can serve as a mechanism for regulating gene expression (60) including the regulation of RNA processing genes (61), our results could also be explained by the apparent loss of the spliceosome in ciDKO podocytes. Indeed, intron retention secondary to mutations in spliceosome components is a hallmark of a number of cancers (62) and neurodegenerative conditions (49). Moreover, it is likely that our RNA seq analysis underestimates the incidence of transcripts with premature termination codons as many will be targeted for nonsense-mediated decay (63) and would thus be unmeasurable in our samples.

Significant differential transcript expression was apparent in ciDKO podocytes with transcripts encoding the extracellular matrix protein fibronectin among the top hits. We detected increased expression of a Fn1 splice variant which included the EDA and EDB exons. Although EDA/EDB-fibronectin is important during development, its expression is limited in adult tissue including kidney (64). However, EDA-fibronectin is upregulated in cultured podocytes exposed to TGFβ treatment (65) and a pathological increase in this isoform results in insulin resistance (66), together with fibrosis in multiple tissues including lung (67) and kidney (68). It is conceivable that the changes in podocyte splicing resulting from IR/IGF1R knockdown promote a fibrotic phenotype by altering the ratio of fibronectin variants expressed, consistent with the increased fibrosis observed in our podDKO mice.

In summary, we have shown that the IR/IGF1R axis is critical for podocyte health. Mechanistically it does this through controlling gene transcription by maintaining spliceosome function. This suggests hormonal signals are important for the genetic control of these terminally differentiated cells.

REFERENCES

1. Tonelli M, Wiebe N, Culleton B, House A, Rabbat C, Fok M, et al. Chronic kidney disease and mortality risk: a systematic review. J Am Soc Nephrol. 2006;17(7):2034-47.
2. Perkovic V, Verdon C, Ninomiya T, Barzi F, Cass A, Patel A, et al. The relationship between proteinuria and coronary risk: a systematic review and meta-analysis. PLoS Med. 2008;5(10):e207.
3. Nakae J, Kido Y, Accili D. Distinct and overlapping functions of insulin and IGF-I receptors. Endocr Rev. 2001;22(6):818-35.
4. Belfiore A, Frasca F, Pandini G, Sciacca L, Vigneri R. Insulin receptor isoforms and insulin receptor/insulin-like growth factor receptor hybrids in physiology and disease. Endocr Rev. 2009;30(6):586-623.
5. Garwood CJ, Ratcliffe LE, Morgan SV, Simpson JE, Owens H, Vazquez-Villasenor I, et al. Insulin and IGF1 signalling pathways in human astrocytes in vitro and in vivo; characterisation, subcellular localisation and modulation of the receptors. Mol Brain. 2015;8:51.
6. Weinstein D, Sarfstein R, Laron Z, Werner H. Insulin receptor compensates for IGF1R inhibition and directly induces mitogenic activity in prostate cancer cells. Endocr Connect. 2014;3(1):24-35.
7. Accili D, Drago J, Lee EJ, Johnson MD, Cool MH, Salvatore P, et al. Early neonatal death in mice homozygous for a null allele of the insulin receptor gene. Nat Genet. 1996;12(1):106-9.
8. Holzenberger M, Dupont J, Ducos B, Leneuve P, Geloen A, Even PC, et al. IGF-1 receptor regulates lifespan and resistance to oxidative stress in mice. Nature. 2003;421(6919):182-7.
9. Boucher J, Softic S, El Ouaamari A, Krumpoch MT, Kleinridders A, Kulkarni RN, et al. Differential Roles of Insulin and IGF-1 Receptors in Adipose Tissue Development and Function. Diabetes. 2016;65(8):2201-13.
10. Li L, Byrd M, Doh K, Dixon PD, Lee H, Tiwari S, et al. Absence of renal enlargement in fructose-fed proximal-tubule-select insulin receptor (IR), insulin-like-growth factor receptor (IGF1R) double knockout mice. Physiol Rep. 2016;4(23).
11. O'Neill BT, Lauritzen HP, Hirshman MF, Smyth G, Goodyear LJ, Kahn CR. Differential Role of Insulin/IGF-1 Receptor Signaling in Muscle Growth and Glucose Homeostasis. Cell Rep. 2015;11(8):1220-35.
12. Soto M, Cai W, Konishi M, Kahn CR. Insulin signaling in the hippocampus and amygdala regulates metabolism and neurobehavior. Proc Natl Acad Sci U S A. 2019;116(13):6379-84.
13. Neirijnck Y, Calvel P, Kilcoyne KR, Kuhne F, Stevant I, Griffeth RJ, et al. Insulin and IGF1 receptors are essential for the development and steroidogenic function of adult Leydig cells. FASEB J. 2018;32(6):3321-35.
14. Coward RJ, Welsh GI, Yang J, Tasman C, Lennon R, Koziell A, et al. The human glomerular podocyte is a novel target for insulin action. Diabetes. 2005;54(11):3095-102.
15. Ising C, Koehler S, Brahler S, Merkwirth C, Hohne M, Baris OR, et al. Inhibition of insulin/IGF-1 receptor signaling protects from mitochondria-mediated kidney failure. EMBO Mol Med. 2015;7(3):275-87.
16. Madhusudhan T, Wang H, Dong W, Ghosh S, Bock F, Thangapandi VR, et al. Defective podocyte insulin signalling through p85-XBP1 promotes ATF6-dependent maladaptive ER-stress response in diabetic nephropathy. Nat Commun. 2015;6:6496.
17. Welsh GI, Hale LJ, Eremina V, Jeansson M, Maezawa Y, Lennon R, et al. Insulin signaling to the glomerular podocyte is critical for normal kidney function. Cell Metab. 2010;12(4):329-40.
18. Bridgewater DJ, Dionne JM, Butt MJ, Pin CL, Matsell DG. The role of the type I insulin-like growth factor receptor (IGF-IR) in glomerular integrity. Growth Horm IGF Res. 2008;18(1):26-37.
19. Bridgewater DJ, Ho J, Sauro V, Matsell DG. Insulin-like growth factors inhibit podocyte apoptosis through the PI3 kinase pathway. Kidney Int. 2005;67(4):1308-14.
20. Hale LJ, Welsh GI, Perks CM, Hurcombe JA, Moore S, Hers I, et al. Insulin-like growth factor-II is produced by, signals to and is an important survival factor for the mature podocyte in man and mouse. J Pathol. 2013;230(1):95-106.
21. Hurcombe JA, Barrington F, Marchetti M, Betin VMS, Bowen EE, Lay AC, et al. Contrasting consequences of podocyte insulin-like growth factor 1 receptor inhibition. iScience. 2024;27(5):109749.

22. Koehler S, Brahler S, Braun F, Hagmann H, Rinschen MM, Spath MR, et al. Construction of a viral T2A-peptide based knock-in mouse model for enhanced Cre recombinase activity and fluorescent labeling of podocytes. Kidney Int. 2017;91(6):1510-7.
23. Maric C, Sandberg K, Hinojosa-Laborde C. Glomerulosclerosis and tubulointerstitial fibrosis are attenuated with 17beta-estradiol in the aging Dahl salt sensitive rat. J Am Soc Nephrol. 2004;15(6):1546-56.
24. Keir LS, Firth R, May C, Ni L, Welsh GI, Saleem MA. Generating conditionally immortalised podocyte cell lines from wild-type mice. Nephron. 2015;129(2):128-36.
25. Saleem MA, O'Hare MJ, Reiser J, Coward RJ, Inward CD, Farren T, et al. A conditionally immortalized human podocyte cell line demonstrating nephrin and podocin expression. J Am Soc Nephrol. 2002;13(3):630-8.
26. Lay AC, Barrington AF, Hurcombe JA, Ramnath RD, Graham M, Lewis PA, et al. A role for NPY-NPY2R signaling in albuminuric kidney disease. Proc Natl Acad Sci U S A. 2020;117(27):15862-73.
27. Hurcombe JA, Hartley P, Lay AC, Ni L, Bedford JJ, Leader JP, et al. Podocyte GSK3 is an evolutionarily conserved critical regulator of kidney function. Nat Commun. 2019;10(1):403.
28. Frankish A, Diekhans M, Jungreis I, Lagarde J, Loveland JE, Mudge JM, et al. Gencode 2021. Nucleic Acids Res. 2021;49(D1):D916-D23.
29. Law CW, Alhamdoosh M, Su S, Dong X, Tian L, Smyth GK, et al. RNA-seq analysis is easy as 1-2-3 with limma, Glimma and edgeR. F1000Res. 2016;5.
30. Robinson MD, McCarthy DJ, Smyth GK. edgeR: a Bioconductor package for differential expression analysis of digital gene expression data. Bioinformatics. 2010;26(1):139-40.
31. Tang AD, Soulette CM, van Baren MJ, Hart K, Hrabeta-Robinson E, Wu CJ, et al. Full-length transcript characterization of SF3B1 mutation in chronic lymphocytic leukemia reveals downregulation of retained introns. Nat Commun. 2020;11(1):1438.
32. Vizcaino JA, Deutsch EW, Wang R, Csordas A, Reisinger F, Rios D, et al. ProteomeXchange provides globally coordinated proteomics data submission and dissemination. Nat Biotechnol. 2014;32(3):223-6.
33. Yokoi A, Kotake Y, Takahashi K, Kadowaki T, Matsumoto Y, Minoshima Y, et al. Biological validation that SF3b is a target of the antitumor macrolide pladienolide. FEBS J. 2011;278(24):4870-80.
34. David JK, Maden SK, Wood MA, Thompson RF, Nellore A. Retained introns in long RNA-seq reads are not reliably detected in sample-matched short reads. Genome Biol. 2022;23(1):240.
35. Prjibelski AD, Mikheenko A, Joglekar A, Smetanin A, Jarroux J, Lapidus AL, et al. Accurate isoform discovery with IsoQuant using long reads. Nat Biotechnol. 2023.
36. White ES, Muro AF. Fibronectin splice variants: understanding their multiple roles in health and disease using engineered mouse models. IUBMB Life. 2011;63(7):538-46.
37. Kim JJ, Park BC, Kido Y, Accili D. Mitogenic and metabolic effects of type I IGF receptor overexpression in insulin receptor-deficient hepatocytes. Endocrinology. 2001;142(8):3354-60.
38. Braun F, Mandel AM, Blomberg L, Wong MN, Chatzinikolaou G, Nair V, et al. Loss of genome maintenance accelerates podocyte damage. 2022:2020.09.13.295303.
39. Braun F, Blomberg L, Akbar-Haase R, Puelles VG, Wong MN, Rahmatollahi M, et al. DNA damage activates mTORC1 signaling in podocytes leading to glomerulosclerosis. 2021:2020.09.13.295303.
40. Hishikawa A, Hayashi K, Abe T, Kaneko M, Yokoi H, Azegami T, et al. Decreased KAT5 Expression Impairs DNA Repair and Induces Altered DNA Methylation in Kidney Podocytes. Cell Rep. 2019;26(5):1318-32 e4.
41. Hayashi K, Hishikawa A, Itoh H. DNA Damage Repair and DNA Methylation in the Kidney. Am J Nephrol. 2019;50(2):81-91.
42. Yoshimoto N, Hayashi K, Hishikawa A, Hashiguchi A, Nakamichi R, Sugita-Nishimura E, et al. Significance of podocyte DNA damage and glomerular DNA methylation in CKD patients with proteinuria. Hypertens Res. 2023.
43. Shkreta L, Chabot B. The RNA Splicing Response to DNA Damage. Biomolecules. 2015;5(4):2935-77.
44. Tam AS, Stirling PC. Splicing, genome stability and disease: splice like your genome depends on it! Curr Genet. 2019;65(4):905-12.

45. Chen L, Chen JY, Huang YJ, Gu Y, Qiu J, Qian H, et al. The Augmented R-Loop Is a Unifying Mechanism for Myelodysplastic Syndromes Induced by High-Risk Splicing Factor Mutations. Mol Cell. 2018;69(3):412-25 e6.
46. Matera AG, Wang Z. A day in the life of the spliceosome. Nat Rev Mol Cell Biol. 2014;15(2):108-21.
47. Yang H, Beutler B, Zhang D. Emerging roles of spliceosome in cancer and immunity. Protein Cell. 2022;13(8):559-79.
48. Nik S, Bowman TV. Splicing and neurodegeneration: Insights and mechanisms. Wiley Interdiscip Rev RNA. 2019;10(4):e1532.
49. Li D, McIntosh CS, Mastaglia FL, Wilton SD, Aung-Htut MT. Neurodegenerative diseases: a hotbed for splicing defects and the potential therapies. Transl Neurodegener. 2021;10(1):16.
50. Griffin C, Saint-Jeannet JP. Spliceosomopathies: Diseases and mechanisms. Dev Dyn. 2020;249(9):1038-46.
51. Zhang Q, Di C, Yan J, Wang F, Qu T, Wang Y, et al. Inhibition of SF3b1 by pladienolide B evokes cycle arrest, apoptosis induction and p73 splicing in human cervical carcinoma cells. Artif Cells Nanomed Biotechnol. 2019;47(1):1273-80.
52. Zhang Y, Yuan Z, Jiang Y, Shen R, Gu M, Xu W, et al. Inhibition of Splicing Factor 3b Subunit 1 (SF3B1) Reduced Cell Proliferation, Induced Apoptosis and Resulted in Cell Cycle Arrest by Regulating Homeobox A10 (HOXA10) Splicing in AGS and MKN28 Human Gastric Cancer Cells. Med Sci Monit. 2020;26:e919460.
53. Suda K, Rozeboom L, Yu H, Ellison K, Rivard CJ, Mitsudomi T, et al. Potential effect of spliceosome inhibition in small cell lung cancer irrespective of the MYC status. PLoS One. 2017;12(2):e0172209.
54. Jorge J, Petronilho S, Alves R, Coucelo M, Goncalves AC, Nascimento Costa JM, et al. Apoptosis induction and cell cycle arrest of pladienolide B in erythroleukemia cell lines. Invest New Drugs. 2020;38(2):369-77.
55. Kim Guisbert KS, Mossiah I, Guisbert E. Titration of SF3B1 Activity Reveals Distinct Effects on the Transcriptome and Cell Physiology. Int J Mol Sci. 2020;21(24).
56. Albert GI, Schell C, Kirschner KM, Schafer S, Naumann R, Muller A, et al. The GYF domain protein CD2BP2 is critical for embryogenesis and podocyte function. J Mol Cell Biol. 2015;7(5):402-14.
57. Lefebvre J, Clarkson M, Massa F, Bradford ST, Charlet A, Buske F, et al. Alternatively spliced isoforms of WT1 control podocyte-specific gene expression. Kidney Int. 2015;88(2):321-31.
58. Stevens M, Oltean S. Modulation of VEGF-A Alternative Splicing as a Novel Treatment in Chronic Kidney Disease. Genes (Basel). 2018;9(2).
59. Stevens M, Oltean S. Alternative Splicing in CKD. J Am Soc Nephrol. 2016;27(6):1596-603.
60. Middleton R, Gao D, Thomas A, Singh B, Au A, Wong JJ, et al. IRFinder: assessing the impact of intron retention on mammalian gene expression. Genome Biol. 2017;18(1):51.
61. Pimentel H, Parra M, Gee SL, Mohandas N, Pachter L, Conboy JG. A dynamic intron retention program enriched in RNA processing genes regulates gene expression during terminal erythropoiesis. Nucleic Acids Res. 2016;44(2):838-51.
62. Dvinge H, Bradley RK. Widespread intron retention diversifies most cancer transcriptomes. Genome Med. 2015;7(1):45.
63. Braunschweig U, Barbosa-Morais NL, Pan Q, Nachman EN, Alipanahi B, Gonatopoulos-Pournatzis T, et al. Widespread intron retention in mammals functionally tunes transcriptomes. Genome Res. 2014;24(11):1774-86.
64. Laitinen L, Vartio T, Virtanen I. Cellular fibronectins are differentially expressed in human fetal and adult kidney. Lab Invest. 1991;64(4):492-8.
65. Madne TH, Dockrell MEC. TGFbeta1-mediated expression and alternative splicing of Fibronectin Extra Domain A in human podocyte culture. Cell Mol Biol (Noisy-le-grand). 2018;64(3):17-24.
66. Gupta S, Ali A, Pandey S, Khan IA, Prakash P. Fibronectin containing alternatively spliced extra domain A interacts at the central and c-terminal domain of Toll-like receptor-4. Sci Rep. 2022;12(1):9662.

67. Muro AF, Iaconcig A, Baralle FE. Regulation of the fibronectin EDA exon alternative splicing. Cooperative role of the exonic enhancer element and the 5' splicing site. FEBS Lett. 1998;437(1-2):137-41.
68. Van Vliet A, Baelde HJ, Vleming LJ, de Heer E, Bruijn JA. Distribution of fibronectin isoforms in human renal disease. J Pathol. 2001;193(2):256-62.

Acknowledgements

We thank the Proteomic Facility and Histology Services Unit at the University of Bristol for technical support. This study was funded by the Medical Research Council (Senior Clinical Fellowship) to RJMC -(MR/K010492/1), Kidney Research UK, and funding from the Innovative Medicines Initiative 2 Joint Undertaking (JU) under grant agreement No 115974. The JU receives support from the European Union's Horizon 2020 research and innovation programme and EFPIA and JDRF. Any dissemination of results reflects only the author's view; the JU is not responsible for any use that may be made of the information it contains.

Author contributions

The study was conceived by R.J.M.C., G.I.W. and J.A.H. Latterly academic input was supplied by M.H. and P.T.B. Experiments were performed by J.A.H., L.D., J.T.C. and F.B. Conditionally immortalised cell lines were made by L.N. PodCre mice were provided by P.T.B. IGF1R $^{fl/fl}$ mice were provided by M.H. Long read RNA sequencing was performed and processed by A.J. and S.B., F.B. bioinformatically analysed and interpreted the data. The manuscript was written by J.A.H and R.J.M.C. and all authors reviewed, commented and approved the paper.

FIGURE LEGENDS

Figure 1. podDKO mice develop a renal phenotype by 24 weeks

A. and **B**. Body weight (**A**) and blood glucose (**B**) are not significantly different in podDKO mice at 24 weeks compared with littermate controls.

C. Urinary Albumin Creatinine ratio (uACR) is significantly increased in podDKO mice at 24 weeks. Unpaired *t*-test, **p<0.01, n=7-8 mice per group.

D. Images and quantification of PAS staining shows tubular protein casts (indicated by arrows) and glomerulosclerosis in podDKO mice. Scale bar=25 µm. Unpaired *t*-test *p<0.05.

E. Masson's trichrome staining shows increased fibrosis (blue staining) in podDKO mice at 24 weeks. Scale bar=25 µm

F. Transmission Electron Micrograph (TEM) images of glomerular filtration barrier (GFB) (scale bar upper panel=5 µm, lower panel=500 nm) show ultrastructural damage to the GFB in podDKO mice with significantly increased foot process width. Unpaired t test **p<0.01

G. Immunofluorescent staining and quantification of WT1 in podDKO and Cre negative control mice at 24 weeks of age shows significant reduction in % podocytes per glomerulus in podDKO mice. Nuclei counterstained with DAPI. Scale bar=100 µm. Unpaired *t*-test ****p<0.0001, ≥8 glomeruli analysed per mouse, 3 mice per group. Scale bar=100 µm.

Figure 2. Simultaneous knockout of podocyte IR and IGF1R *in vitro* is highly detrimental

A. Western blot shows >80% reduction of IR and IGF1R protein in ciDKO cells. *t*-test, ****p<0.00001, n=18.

B. Phosphorylation of AKT and p44/42MAPK in response to acute insulin stimulation at 10 nM and 100 nM for 10 minutes was significantly reduced in ciDKO podocytes. One way ANOVA, **p<0.01, *p<0.05, n=3.

C. Phosphorylation of AKT and p44/42MAPK in response to acute IGF1 stimulation at 10 and 100 ng/ml for 10 minutes was reduced in ciDKO podocytes. One way ANOVA, *p<0.05, n=3.

D. Fewer than 50% of ciDKO cells survive 7 days after gene excision. *t*-test, ****p<0.0001, n=3-4 independent experiments.

Figure 3. Proteomic analysis of ciDKO podocytes reveals downregulation of spliceosomal proteins

A. Schematic outlining workflow for proteomic analysis.

B. Heat map showing hierarchical clustering of ciDKO vs wild-type podocyte proteomes (decreased protein expression in green, increased expression in red) and the GO and KEGG terms enriched in four major clusters.

C. and **D.** KEGG enriched terms in STRING. Downregulated pathways (green) are associated with higher enrichment scores in comparison to upregulated pathways (red). Enrichment scores are computed by STRING using the Kolmogorov-Smirnoff test. KEGG term "Spliceosome" (highlighted border) is associated with a high enrichment score and the highest false discovery rate across all terms.

E. Western blots show significantly reduced levels of EIF4A, SF3B4 and PTBP2 in ciDKO podocytes compared with wild-type cells. Unpaired *t*-test, ***p<0.001, **p<0.01, *p<0.05, n=3 independent experiments.

Figure 4. Exposure of cultured podocytes, but not glomerular endothelial cells, to the spliceosome inhibitor pladienolide B results in dose dependent cell death

A. Annotated KEGG pathway showing a majority of spliceosome proteins are significantly downregulated (green) in ciDKO podocytes.

B-D. Pladienolide B exposure for 48 hours in HeLa cells (**B**), glomerular endothelial cells (GenC) (**C**) and podocytes (**D**). One way ANOVA, ****p<0.0001, **p<0.01, *p<0.05, n=3 independent experiments.

E. Bright field images of wild-type podocytes exposed to the indicated concentrations of pladienolide B. Scale bar=100 µm

Figure 5. Loss of podocyte IR and IGF1R is associated with increases in intron retention and unproductive transcript expression

A. Schematic outlining long read RNA sequencing workflow

B. An overview of the alternative splicing events quantified by FLAIR. Boxes represent exons (blue=constitutive exons; yellow=alternative exons), lines represent introns.

C. Boxplot showing the fraction of transcripts with intron retention events in ciDKO and wild-type podocytes. *t*-test, **p<0.01, n=4 for each experimental condition.

D. Box plot of the fraction of productivity events in the ciDKO and wild-type transcriptomes shows a higher proportion of unproductive transcripts in ciDKO podocytes. NGO=no start codon; NST=start codon but no stop codon; PRO=productive transcripts; PTC=premature termination codon ie. unproductive transcripts. *t*-test, ***p<0.001, **p<0.01, *p< 0.05, n=4 for each experimental condition.

E. Proportional stacked bar graph of productivity events in the ciDKO and wild-type transcriptomes. NGO=no start codon; NST=start codon but no stop codon; PRO=productive transcripts; PTC=premature termination codon ie. unproductive transcripts.

Figure 6. Compound knockdown of the IR and IGF1R alters the podocyte transcriptome

A. UCSC genome browser tracks of transcripts annotated to *Fn1.* Red lines indicate the number of reads in each sample containing the EDA and EDB exons.

B. Boxplot showing differential expression of an Fn1 transcript containing EDA/EDB exons in ciDKO podocytes.

C. Exon/intron structure of Fn1 transcript differentially expressed in IGF1R DKO vs wild-type podocytes. Expression of an EDA and EDB exon-containing transcript (not normally expressed in mature podocytes and associated with fibrosis) is increased in IGF1R DKO podocytes.

D. qPCR using primers specific to the Fn1 EDB exon shows an increase in the expression of fibrosis associated EDB exon-containing transcripts in ciDKO podocytes. *t*-test, **p<0.001, n=4 independent experiments.

E. qPCR shows decreased expression of Hcfc1r1 mRNA in ciDKO podocytes. *t*-test, ****p<0.00001, n=4 independent experiments.

Figure 1

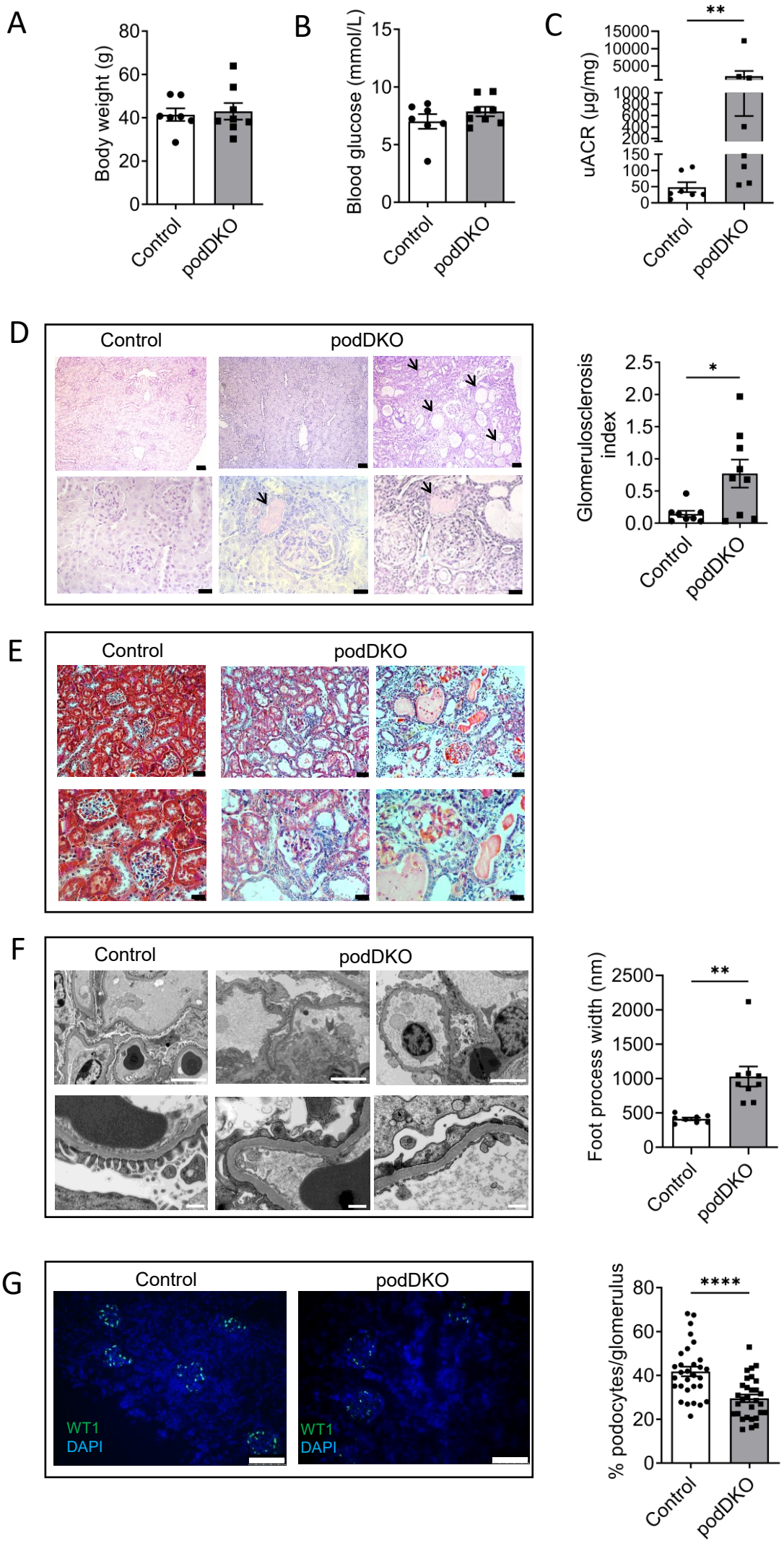
A
Body weight (g)
80
60
40
20
0
Control
podDKO
B
Blood glucose (mmol/L)
15
10
5
0
Control
podDKO
C
uACR (µg/mg)
**
15000
10000
5000
1000
800
600
400
200
150
100
50
0
Control
podDKO
D
Control
podDKO
Glomerulosclerosis index
*
2.5
2.0
1.5
1.0
0.5
0.0
Control
podDKO
E
Control
podDKO
F
Control
podDKO
Foot process width (nm)
**
2500
2000
1500
1000
500
0
Control
podDKO
G
Control
podDKO
WT1
DAPI
WT1
DAPI
% podocytes/glomerulus
****
80
60
40
20
0
Control
podDKO

Figure 2

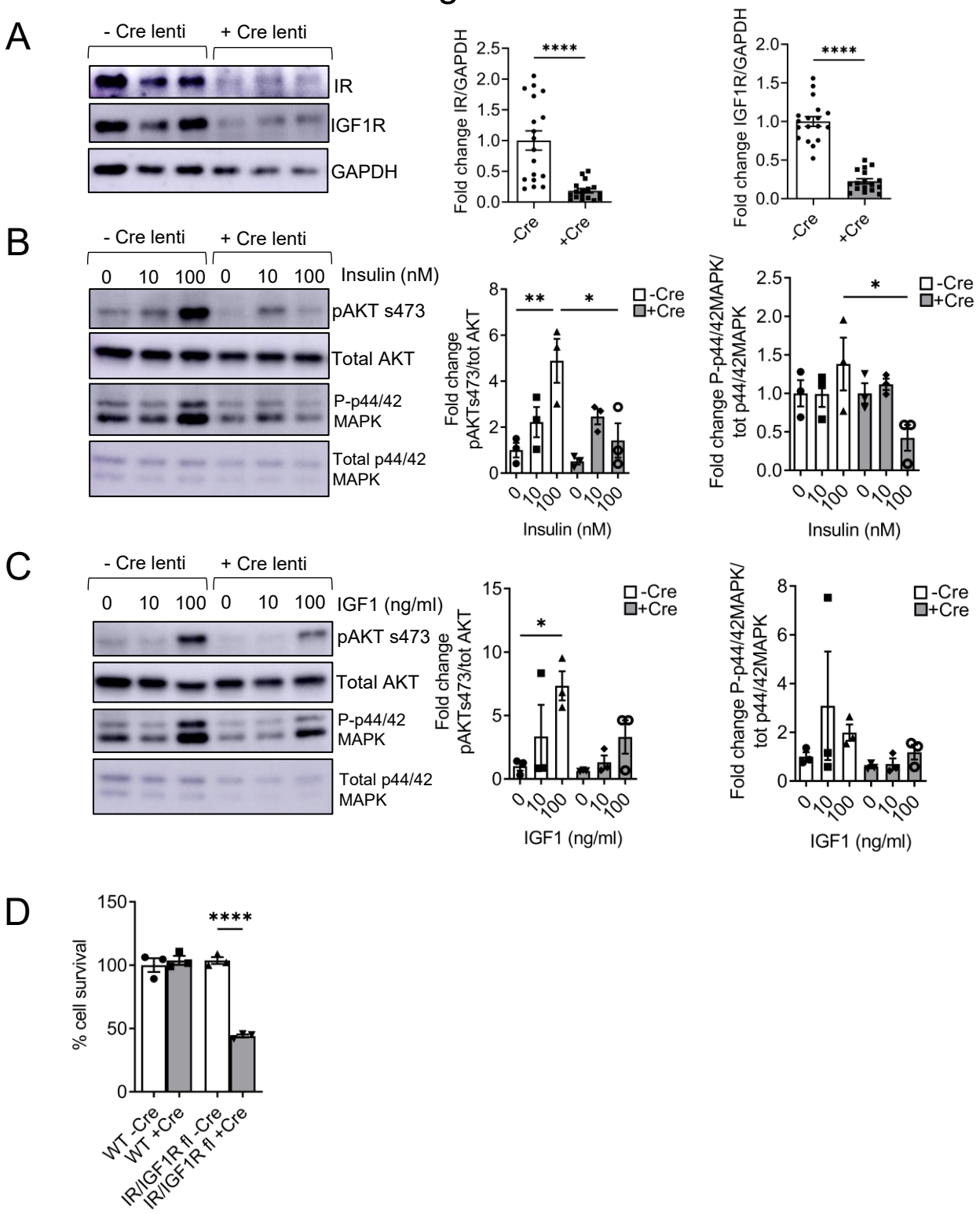
A
- Cre lenti
+ Cre lenti
IR
IGF1R
GAPDH
Fold change IR/GAPDH
Fold change IGF1R/GAPDH
****
-Cre
+Cre
B
- Cre lenti
+ Cre lenti
0 10 100 0 10 100
Insulin (nM)
pAKT s473
Total AKT
P-p44/42 MAPK
Total p44/42 MAPK
Fold change pAKTs473/tot AKT
Fold change P-p44/42MAPK/ tot p44/42MAPK
**
*
-Cre
+Cre
Insulin (nM)
C
- Cre lenti
+ Cre lenti
0 10 100 0 10 100
IGF1 (ng/ml)
pAKT s473
Total AKT
P-p44/42 MAPK
Total p44/42 MAPK
Fold change pAKTs473/tot AKT
Fold change P-p44/42MAPK/ tot p44/42MAPK
*
-Cre
+Cre
IGF1 (ng/ml)
D
% cell survival
****
WT -Cre
WT +Cre
IR/IGF1R fl -Cre
IR/IGF1R fl +Cre

Figure 3

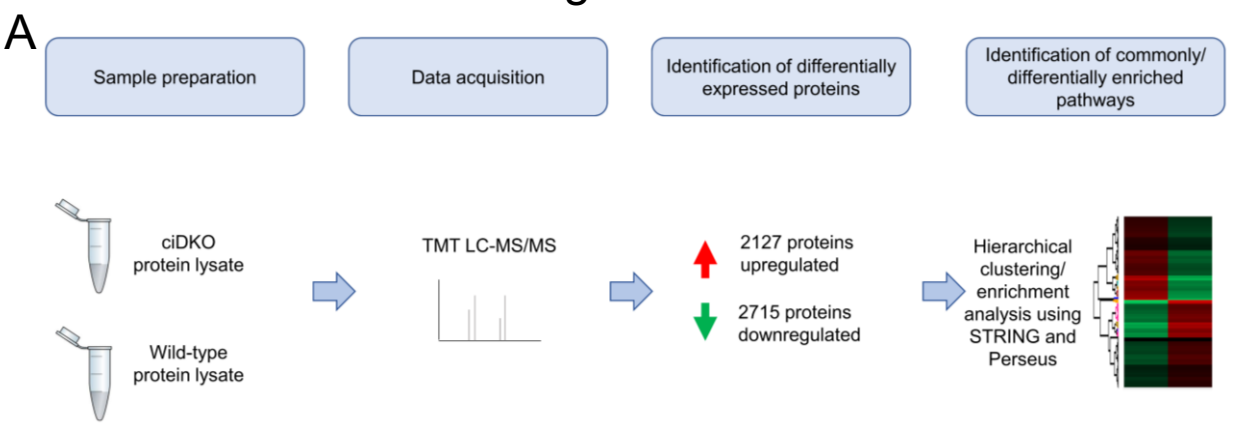
A
Sample preparation
Data acquisition
Identification of differentially expressed proteins
Identification of commonly/ differentially enriched pathways
ciDKO protein lysate
Wild-type protein lysate
TMT LC-MS/MS
2127 proteins upregulated
2715 proteins downregulated
Hierarchical clustering/ enrichment analysis using STRING and Perseus

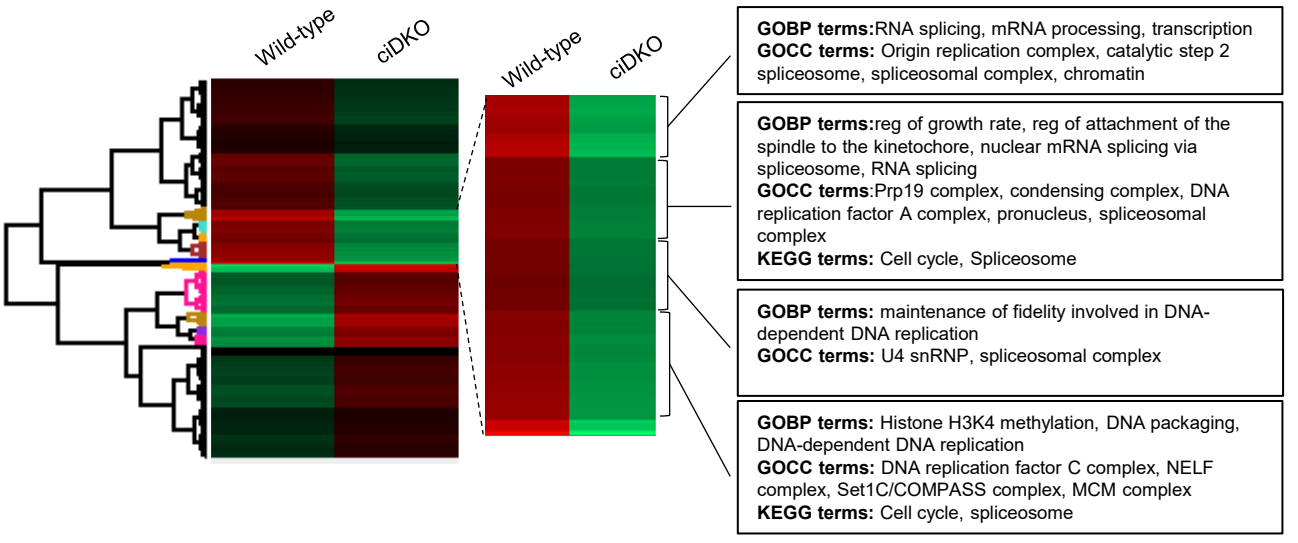
B
Wild-type
ciDKO
Wild-type
ciDKO
GOBP terms:RNA splicing, mRNA processing, transcription
GOCC terms: Origin replication complex, catalytic step 2 spliceosome, spliceosomal complex, chromatin
GOBP terms:reg of growth rate, reg of attachment of the spindle to the kinetochore, nuclear mRNA splicing via spliceosome, RNA splicing
GOCC terms:Prp19 complex, condensing complex, DNA replication factor A complex, pronucleus, spliceosomal complex
KEGG terms: Cell cycle, Spliceosome
GOBP terms: maintenance of fidelity involved in DNA-dependent DNA replication
GOCC terms: U4 snRNP, spliceosomal complex
GOBP terms: Histone H3K4 methylation, DNA packaging, DNA-dependent DNA replication
GOCC terms: DNA replication factor C complex, NELF complex, Set1C/COMPASS complex, MCM complex
KEGG terms: Cell cycle, spliceosome

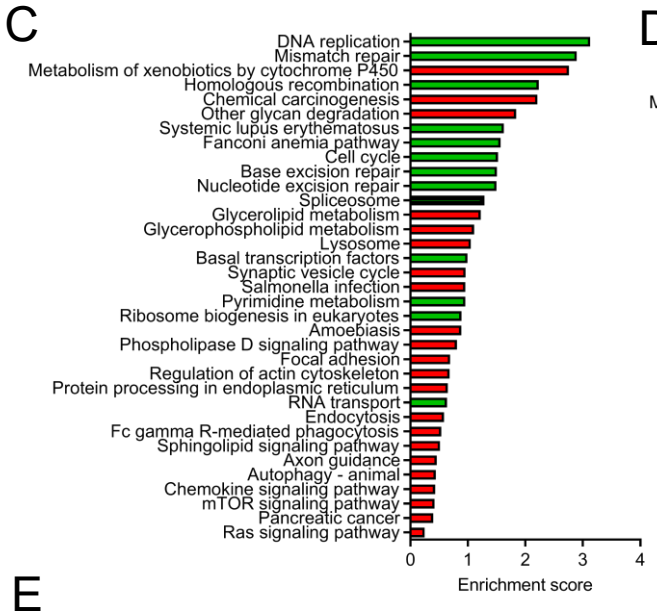
C
DNA replication
Mismatch repair
Metabolism of xenobiotics by cytochrome P450
Homologous recombination
Chemical carcinogenesis
Other glycan degradation
Systemic lupus erythematosus
Fanconi anemia pathway
Cell cycle
Base excision repair
Nucleotide excision repair
Spliceosome
Glycerolipid metabolism
Glycerophospholipid metabolism
Lysosome
Basal transcription factors
Synaptic vesicle cycle
Salmonella infection
Pyrimidine metabolism
Ribosome biogenesis in eukaryotes
Amoebiasis
Phospholipase D signaling pathway
Focal adhesion
Regulation of actin cytoskeleton
Protein processing in endoplasmic reticulum
RNA transport
Endocytosis
Fc gamma R-mediated phagocytosis
Sphingolipid signaling pathway
Axon guidance
Autophagy - animal
Chemokine signaling pathway
mTOR signaling pathway
Pancreatic cancer
Ras signaling pathway
0
1
2
3
4
Enrichment score

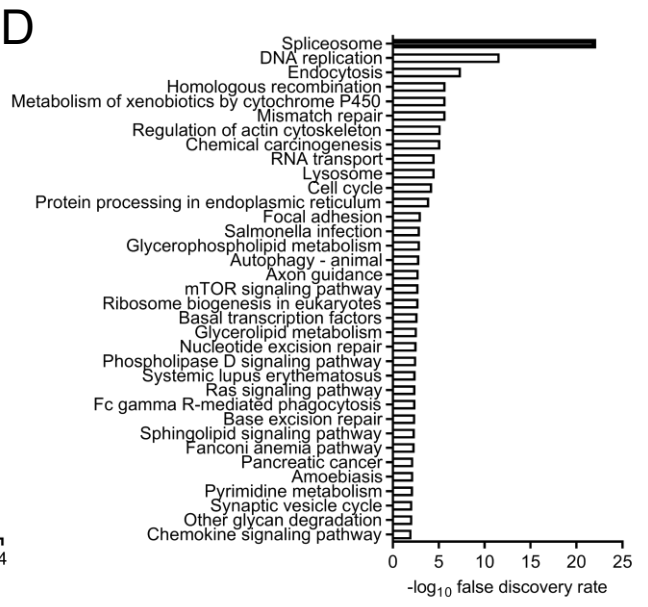
D
Spliceosome
DNA replication
Endocytosis
Homologous recombination
Metabolism of xenobiotics by cytochrome P450
Mismatch repair
Regulation of actin cytoskeleton
Chemical carcinogenesis
RNA transport
Lysosome
Cell cycle
Protein processing in endoplasmic reticulum
Focal adhesion
Salmonella infection
Glycerophospholipid metabolism
Autophagy - animal
Axon guidance
mTOR signaling pathway
Ribosome biogenesis in eukaryotes
Basal transcription factors
Glycerolipid metabolism
Nucleotide excision repair
Phospholipase D signaling pathway
Systemic lupus erythematosus
Ras signaling pathway
Fc gamma R-mediated phagocytosis
Base excision repair
Sphingolipid signaling pathway
Fanconi anemia pathway
Pancreatic cancer
Amoebiasis
Pyrimidine metabolism
Synaptic vesicle cycle
Other glycan degradation
Chemokine signaling pathway
0
5
10
15
20
25
-log10 false discovery rate

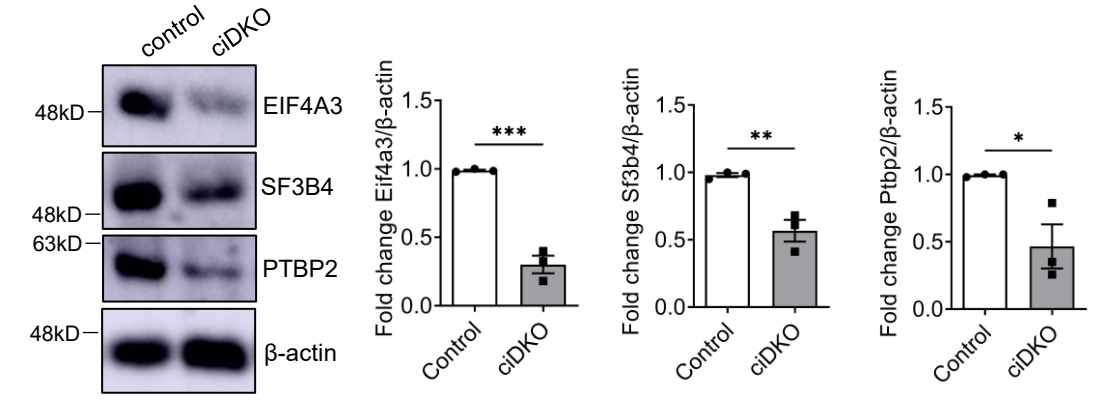
E
control
ciDKO
48kD
EIF4A3
48kD
SF3B4
63kD
PTBP2
48kD
β-actin
Fold change Eif4a3/β-actin
1.5
1.0
0.5
0.0
***
Control
ciDKO
Fold change Sf3b4/β-actin
1.5
1.0
0.5
0.0
**
Control
ciDKO
Fold change Ptbp2/β-actin
1.5
1.0
0.5
0.0
*
Control
ciDKO

Figure 4

A

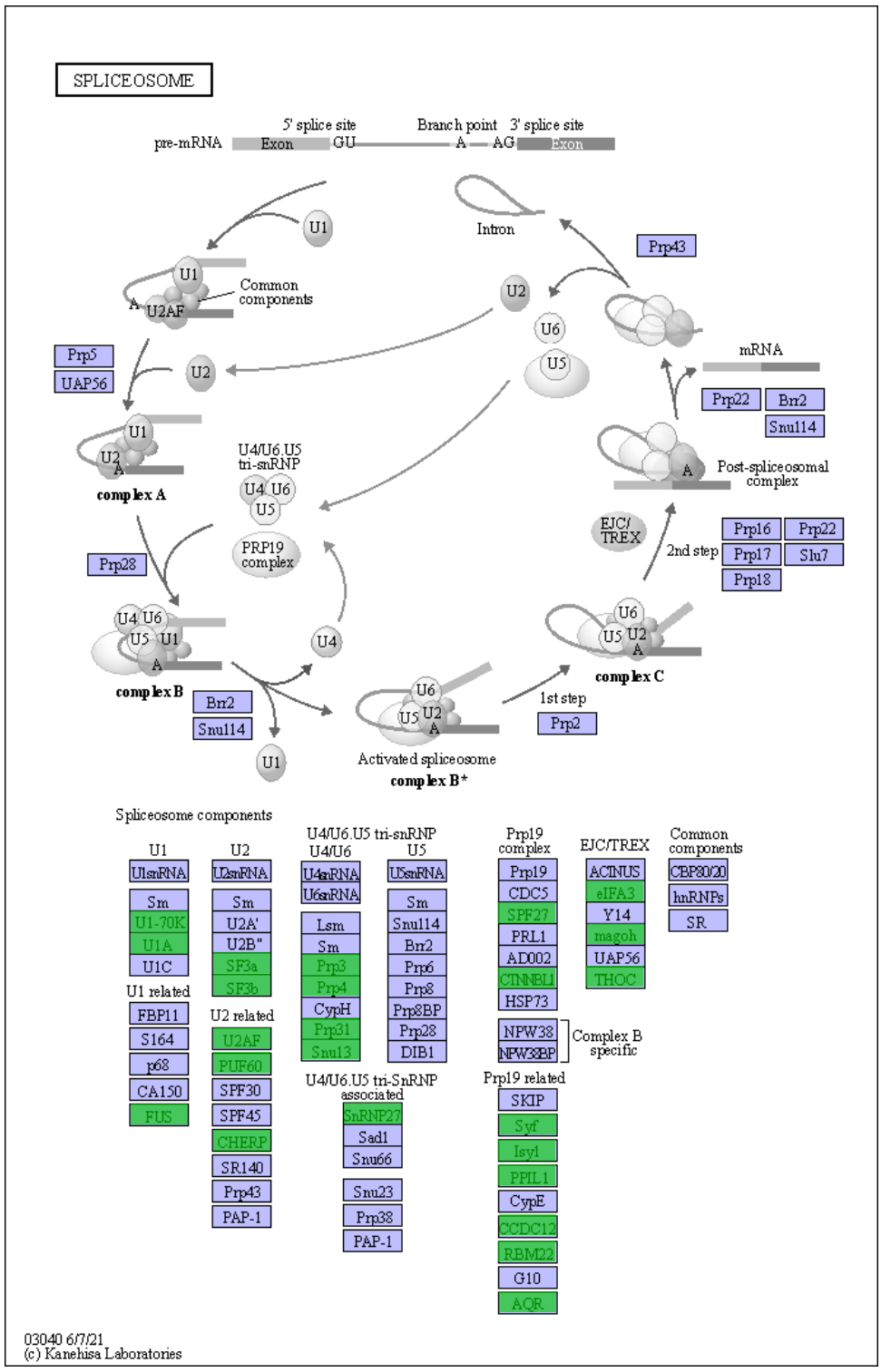

B

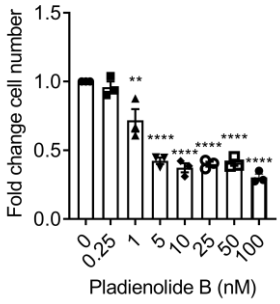

C

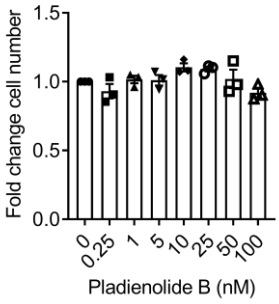

D

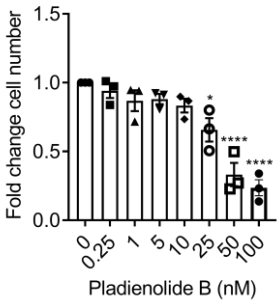

E

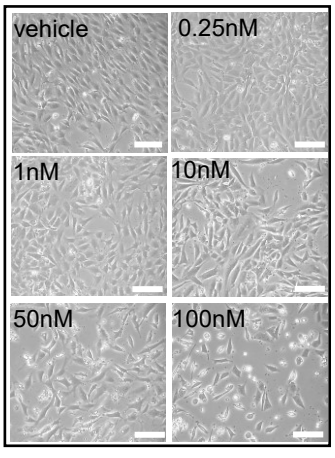

Figure 5

A

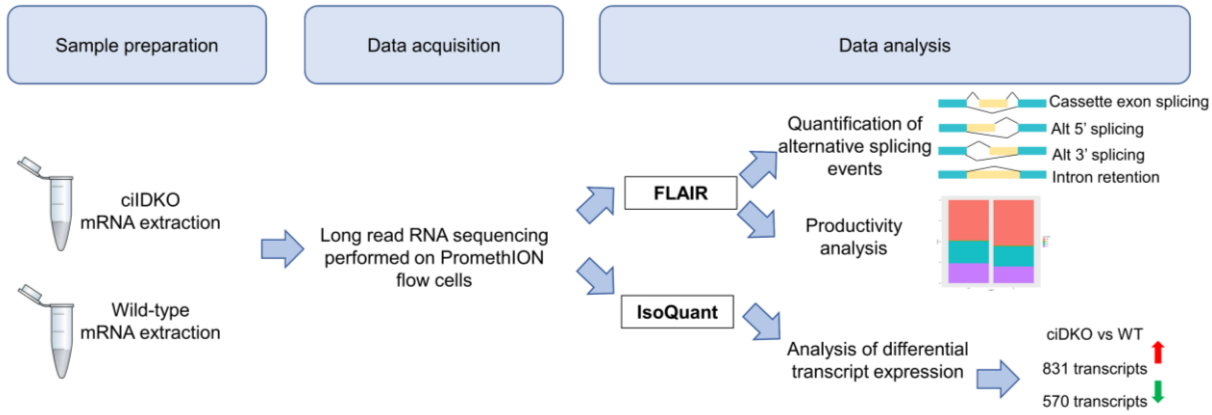

B

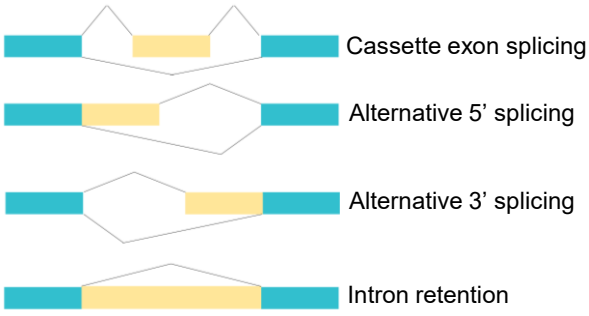

C

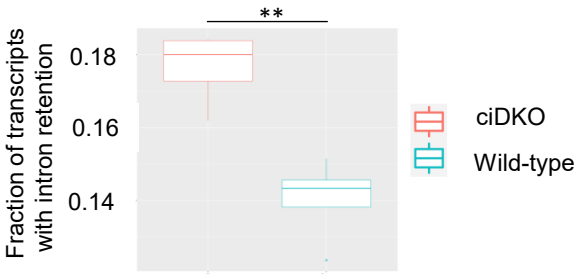

D

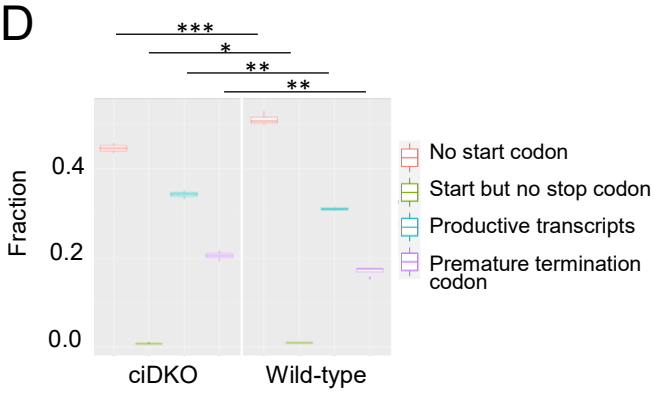

E

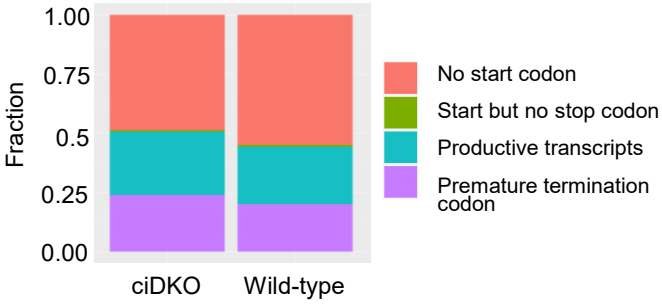

Figure 6

A

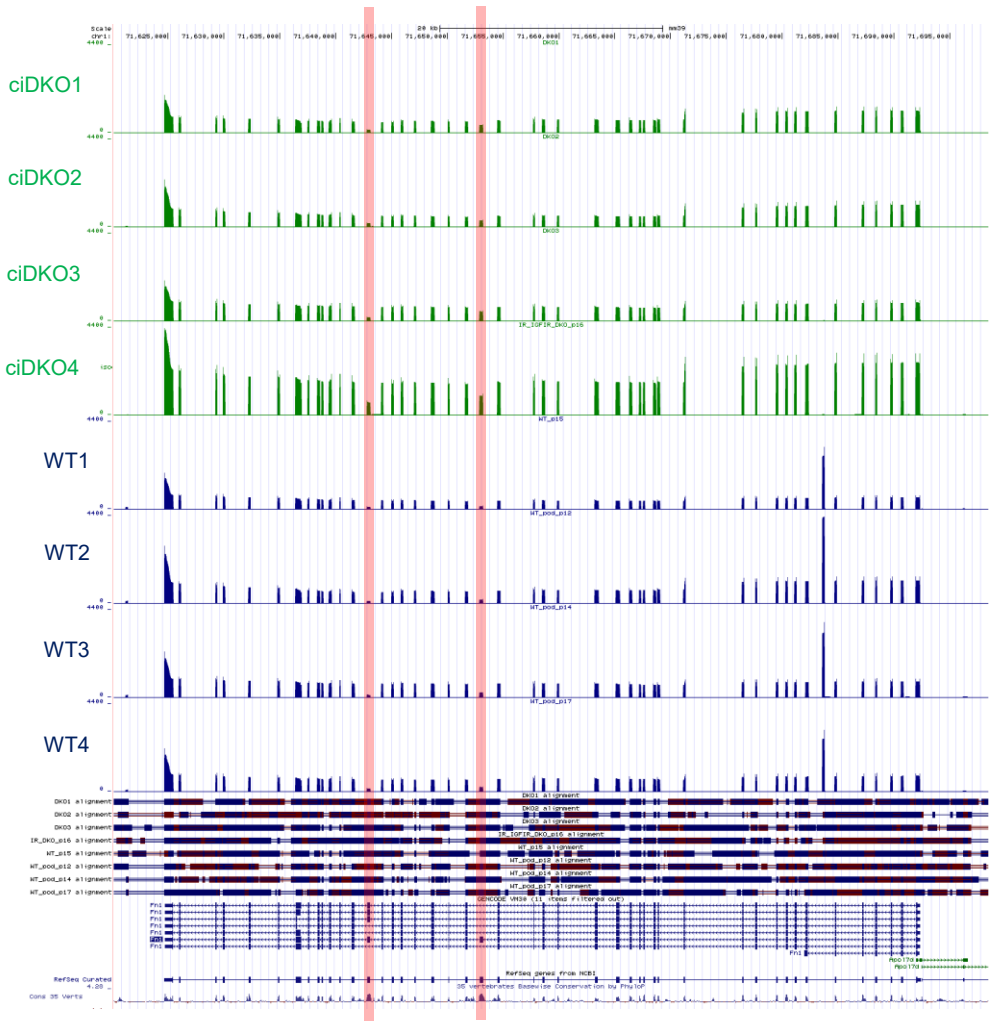

B

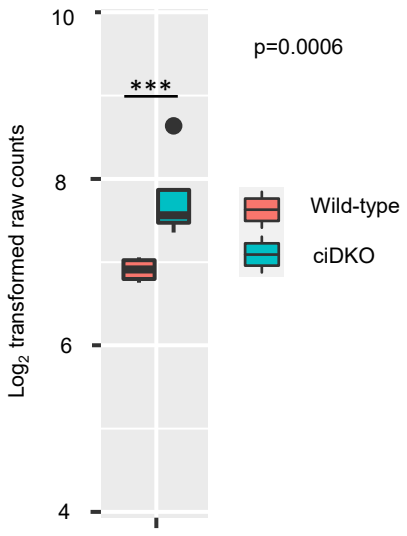

C

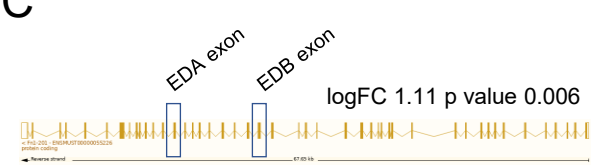

D

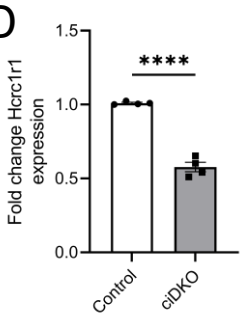
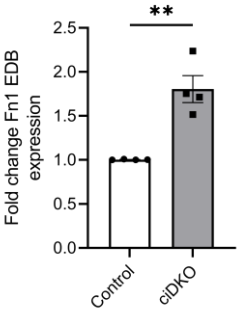
E